Selection Metric for Photovoltaic Materials Screening Based on Detailed-Balance Analysis

Beatrix Blank, Thomas Kirchartz, Stephan Lany, and Uwe Rau

Phys. Rev. Applied **8**, 024032 — Published 31 August 2017

DOI: 10.1103/PhysRevApplied.8.024032

Selection metric for photovoltaic materials screening based on detailed balance analysis

Beatrix Blank,[1] Thomas Kirchartz,[1,2] Stephan Lany,[3] and Uwe Rau[1]

[1]IEK5-Photovoltaics, Forschungszentrum Jülich, 52425 Jülich, Germany

[2]Faculty of Engineering and CENIDE, University of Duisburg-Essen, Carl-Benz-Str. 199, 47057 Duisburg, Germany

[3]National Renewable Energy Laboratory, Golden, Colorado 80401, USA

Abstract

The success of recently discovered absorber materials for photovoltaic applications has been generating an increasing interest in systematic materials screening over the last years. However, the key for a successful materials screening is a suitable selection metric that goes beyond the Shockley-Queisser theory that determines the thermodynamic efficiency limit of an absorber material solely by its band gap energy. In this work, we develop a selection metric to quantify the potential photovoltaic efficiency of a material. Our approach is compatible with detailed balance and applicable in computational and experimental materials screening. We use the complex refractive index to calculate radiative and non-rradiative efficiency limits and the respective optimal thickness in the high mobility limit. We compare our model to the widely applied selection metric by Yu and Zunger [Phys Rev Lett **108**, 068701 (2012)] with respect to their dependency on thickness, internal luminescence quantum efficiency and refractive index. Finally the model is applied to complex refractive indices calculated via electronic structure theory.

I. Introduction

Due to the wide variety of potential absorber materials for photovoltaic applications including organic and inorganic materials as well are organic-inorganic compounds like the recently developed perovskite solar cells there has been a growing interest to find new photovoltaic absorber materials via computational but also experimental materials screening in recent years [1-14]. The purpose of materials screening is to identify promising materials for more in-depth investigations based on a limited amount of information on the material. For a given purpose such as photovoltaics, it is therefore crucial to decide what information on a material is needed to make well informed decisions in a finite amount of time. This requires a suitable "selection metric" for promising absorber materials for photovoltaic applications that goes beyond the radiative efficiency limit as calculated by Shockley and Queisser (SQ) [15]. The SQ approach describes a solar cell exclusively by an external property, the step-like absorption $A(E) = \Theta\left(E - E_{\mathrm{g}}\right)$. Thus, the radiative efficiency limit depends on one parameter only: the band gap energy E_{g}.

It is apparent that exclusively considering the band gap energy of a material is not sufficient to estimate its potential as an absorber material. Numerous other properties such as the mobility [16, 17], the absorption coefficient [18, 19], the charge-carrier lifetime [18-20], and the luminescence quantum efficiency [21-27] have an enormous effect on a solar cell's performance. Hence, there have been various studies to calculate a more realistic efficiency limit beyond the SQ limit for different technologies and assumptions [18, 19, 28-36].

One of the first and maybe most prominent examples of such a selection metric proposed for computational materials screening is presented by Yu and Zunger in 2012 [37] and has been widely used to estimate efficiency limits in the last years [38-49]. In their paper, they proposed a "spectroscopic

limited maximum efficiency" SLME selection metric that aims to calculate efficiency limits for non-step like absorption coefficients beyond the radiative limit. They calculate the efficiency in the high mobility limit using absorption coefficients simulated via electronic structure theory. While the SLME takes non-radiative recombination into account, the paper does not distinguish between internal Q_{i} and external luminescence yield Q_e, i.e. the number of photons generated in the device via radiative recombination are set equal to the number of photons that subsequently escape the device, and is therefore only correct in the limit of perfect light outcoupling, a limit that does not apply to realistic devices.

The present paper proposes a modified selection metric based on Ref. [24] that is detailed-balance compatible and takes effects of light outcoupling, photon recycling and non-radiative recombination into account. As illustrated by Figure 1, the complex refractive index, the device thickness, and the light trapping structure represents the *minimum* parameter set needed for a physically consistent approximation of the efficiency potential of a photovoltaic absorber material defined by bulk material properties and not by the band gap energy only. This step takes us from a description of the solar cell as a *surface* specified by a stepfunction like absorptance in the SQ-approach to a solar cell specified by *bulk* properties. This minimum parameter set allows us to calculate the (non-step function) absorptance and herewith the radiative limit, see Figure 1. We emphasize that there is no other intermediate step possible and any sophistication of the SQ-approach needs to consider at least this parameter set in order to be physically consistent.

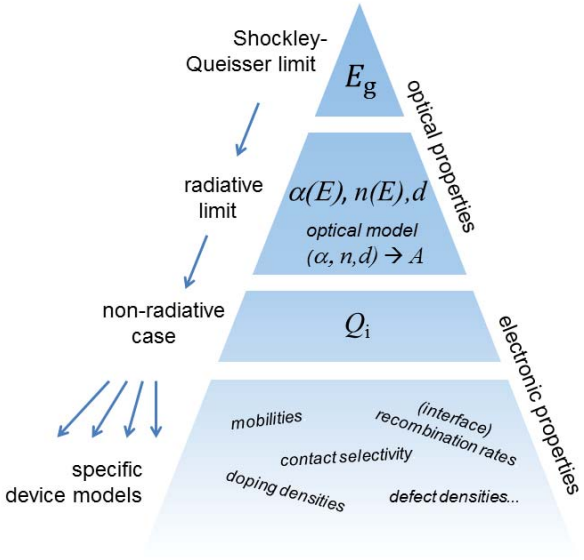

Figure 1: *The SQ-limit is derived using an approximation that is parametrized by the band gap energy E_g only. Steps towards more detail must be undertaken in the order from top to down. Any model describing the radiative limit as a function of material properties must contain the absorption coefficient $\alpha(E)$ and the refractive index n(E) as well as assumptions on the device thickness and an optical model for light trapping. The next step involves non-radiative recombination, i.e. an internal luminescence quantum efficiency $Q_i < 1$. Generic device models considering finite mobilities, interface recombination, or contact selectivity must involve the first two steps in order to be compatible with the SQ-approach. Note that the standard device simulations for real photovoltaic devices usually involve hundreds of material specific parameters.*

The next step towards more detail in this top-down approach is the inclusion of non-radiative recombination in terms of an internal luminescence quantum efficiency leading us to a generic non-radiative case. Notably, we shift then from optical properties towards electronic properties. Within the

present paper, we restrict ourselves to this level of detail, whereas one might think about the selectivity of contacts [50] and the influence of carrier mobilities [16] as the logical next levels of detail, which are still far more generic than detailed device models.

We note that the procedure proposed here corresponds to the way how e.g., Tiedje et al. have calculated the efficiency limit for crystalline silicon solar cells [51], how Marti et al. have explained the importance of photon recycling [52], how Mattheis et al. have calculated the radiative mobility limits of photovoltaic energy conversion [53], and how the impact of a direct/indirect band gap on the efficiency potential of metal-halide perovskites was evaluated[54]. Thus, the issue of the present paper is to systematically describe what all these authors (and many others) have done right and therewith to establish a canonical, detailed balance compatible top-down approach. This approach serves as a guideline, and finally a recipe, on how to conduct and correctly interpret first principle calculations for new photovoltaic materials.

We will demonstrate this method by applying it to different materials whose complex refractive index has been calculated by first principles calculations in the so-called GW approximation [55] in the radiative limit (internal luminescence quantum efficiency $Q_{\mathrm{i}} = 1$). In addition, we highlight how sensitive the efficiency limit reacts on non-radiative recombination, i.e. when Q_{i} is reduced. The approach proposed here will be useful both for computational materials screening in photovoltaics but also for experimental materials screening where properties of absorber layers are used to determine the efficiency potential of a certain material class [20, 56, 57].

II. Theory

a. Shockley-Queisser limit

Shockley and Queisser were the first to determine thermodynamic efficiency limits based on the principle of detailed balance. The short-circuit current in the Shockley-Queisser (SQ) limit is written as

$$J_{\mathrm{SC}} = q \int_0^{\infty} A(E)\ \phi_{\mathrm{sun}}(E)\, dE, \tag{1}$$

where E is the energy, q the elementary charge, and the absorptance $A(E)$ is assumed to be step-function at the band gap energy E_{g} defined as $A(E) = 0$ for $E \leq E_{\mathrm{g}}$, and $A(E) = 1$ for $E > E_{\mathrm{g}}$. Whereas in the original paper by Shockley and Queisser, the spectrum of the sun is approximated by the black body spectrum at temperature *T* = 6000K, in this work we use the AM1.5g [58] spectrum as it is common nowadays. The radiative saturation current can be calculated via

$$J_0^{\mathrm{rad}} = q \int_0^{\infty} A(E)\ \phi_{\mathrm{bb}}(E,\ T = 300K)\, dE. \tag{2}$$

The black body spectrum at temperature *T* is given by $\phi_{\mathrm{bb}}(E,T) = 2E^2 \mathrm{h}^{-3}\mathrm{c}^{-2}\left(\exp\left(\frac{E}{kT}\right) - 1\right)^{-1}$ where h denotes the Planck constant, c the velocity of light in vacuum and k the Boltzmann constant. Assuming an ideality factor of $n_{\mathrm{id}} = 1$ the efficiency limit η (in the radiative limit η^{rad}, i.e. internal luminescence quantum efficiency $Q_{\mathrm{i}} = 1$) is given by

$$\eta^{(\mathrm{rad})} = \frac{\max\limits_V \left[V \cdot \left[J_{\mathrm{SC}} - J_0^{(\mathrm{rad})}\left(\exp\left(\frac{qV}{kT}\right) - 1\right)\right]\right]}{\int_0^{\infty} E\ \phi_{\mathrm{sun}}(E)\, dE}, \tag{3}$$

where V is the voltage of the solar cell.

Shockley and Queisser consider only one material property, the band gap energy E_{g}, by assuming a step-like absorption. However, the simplicity achieved by the step function forces Shockley and Queisser to implicitly assume that the solar cell absorber is both infinitely thick (to achieve the step function) and infinitely thin at the same time (because perfect charge carrier collection is another inherent assumption of Shockley and Queisser) [59]. Therefore a generalization of the SQ theory [31-33] is

needed to adapt this approach to a realistic scenario and finally define a suitable selection metric for computational and experimental materials screening.

b. Extended detailed balance theory

The original SQ-theory is in general straightforward to generalize because Equations (1)-(3) are also valid for non-step-function like absorptances, thereby allowing for the calculation of the radiative efficiency limit of real materials [18, 19, 33, 35, 56]. For computational materials screening however we have to go one step further, by connecting the internal material properties with external device properties. This has frequently not been implemented correctly and has led to confusion and mistakes in the past [37-49]. The internal and external parameters used in the scope of this work are listed in Table I as well as the equations that connect an internal parameter with its external counterpart.

One example of an internal parameter would be the complex refractive index, which describes the optical properties of the material. The corresponding external parameter would be the absorptance $A(E)$ which depends e.g. on the complex refractive index (or the absorption coefficient), the thickness and the scattering properties of the interfaces (flat or textured). Another example is the recombination rates and the recombination currents. Whereas the rates describe recombination per volume and time, the currents are the integrated rates per area and time and in case of the radiative recombination current also include the percentage of photons that are coupled out of the device and are not reabsorbed in the solar cell. Therefore, the recombination currents and in consequence the external luminescence quantum efficiency Q_{e} depend on outcoupling and optical properties of the device whereas the internal quantum efficiency Q_{i} depends primarily on the properties of the material (electron-photon and electron-phonon coupling). Note that in case of geometric features on the size of the wavelength, interference effects can modify the spontaneous emission rate and thereby Q_{i} (Purcell effect) [60, 61].

It is clear that materials screening will provide internal parameters while efficiency estimates require external properties. Any sensible selection metric, therefore, has to find a way to self-consistently and correctly calculate external parameters from internal parameters. Figure 2 illustrates the "internal material world" and the "external device world" where the solar cell is treated as a black box with optical and electrical in and output. The connection between the internal and the external picture is light in- and outcoupling, i.e. optics, and will in the following be described consistently with the principle of detailed balance.

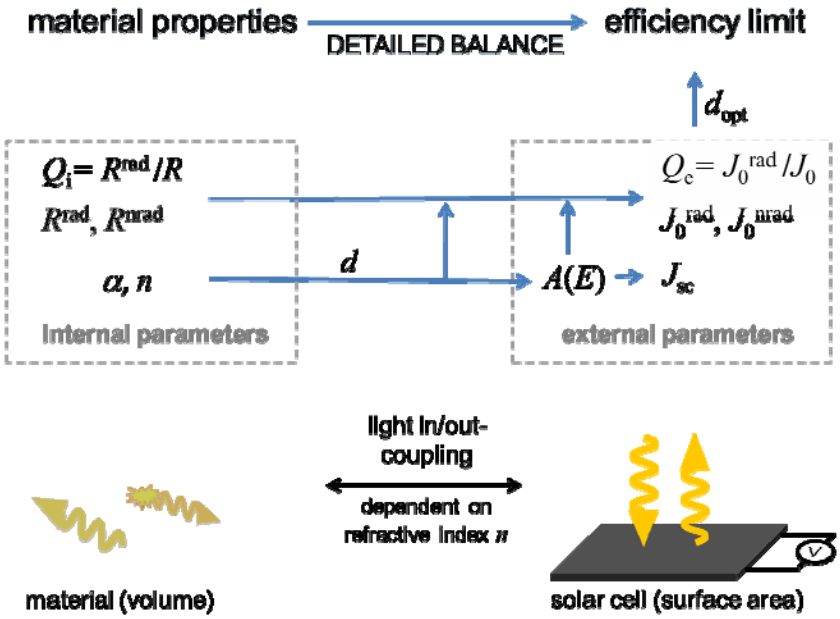

Figure 2: *Illustration of the internal material description (via volume related material properties) and the external device description (via area related cell properties) of a solar cell. On the left the path of the photons inside the volume of the cell and their interaction with electron-hole pairs are considered, on the right side the light and current are described as in- and output parameters of a solar cell device. For the calculation of the efficiency limit of a device from material properties(absorption coefficient α, refractive index n, radiative recombination rate R^{rad}, non-radiative recombination rate R^{nrad}, internal luminescence quantum efficiency Q_i) towards external variables (short circuit current density J_{sc}, radiative saturation*

current density J_0^{rad},non-radiative saturation current density J_0^{nrad}, external luminescence quantum efficiency Q_e) these two descriptions have to be carefully connected. The maximum device efficiency is obtained by assuming a specific light trapping scheme and optimizing the cell thickness d.

Table I: *Internal vs. external parameter. Note that the radiative and non-radiative recombination rates are defined here as the recombination rates in thermodynamic equilibrium.*

INTERNAL PARAMETER				EXTERNAL PARAMETER
absorption coefficient	α	$1-\exp(-2\alpha d)$ (e.g. flat cell, Lambert-Beer Approximation)	$=$ $A(E)$	absorptance
non-radiative recombination rate	R_0^{nrad}	$q\int R_0^{\mathrm{nrad}}dx$	$=$ J_0^{nrad}	non-radiative saturation current density
radiative recombination rate	R_0^{nrad}	$p_{\mathrm{e}}\, q\int R_0^{\mathrm{rad}}dx$	$=$ J_0^{rad}	radiative saturation current density
internal (luminescence) quantum efficiency	Q_{i}	$\frac{p_{\mathrm{e}}Q_{\mathrm{i}}}{1+(p_{\mathrm{e}}-1)Q_{\mathrm{i}}}$	$=$ Q_{e}	external luminescence quantum efficiency

At first, the external property, the absorptance $A(E)$, needs to be computed from the absorption coefficient $\alpha(E)$, a volume related internal property of the photovoltaic absorber material. This requires assumptions on the thickness *d* and on the applied light trapping scheme [18, 62]. In this work, we apply two different light trapping schemes. The first model represents the case of a solar cell with flat front and back surfaces. For simplicity, the reflectance at the front surface is set to zero and the reflectance at the back is assumed to be unity. The complex refractive indices of the materials are considered to be homogeneous and isotropic. Moreover we neglect any interference effecs such as resonator modes. For a more detailed description and the respective equation see the supplemental material [54]. The second model is identical with respect to the assumptions on reflectance, optical isotropy and homogeniety, but

it assumes a Lambertian scatterer at the front surface. In this case, we use the analytical solution via the exponential integral function introduced by Green [63].

A similar step from volume to surface properties with careful distinction between internal and external parameters is required for the description of recombination. Here the internal volume parameters are the radiative and non-radiative recombination rates R^{rad} and R^{nrad} defining the internal luminescence quantum efficiency as follows

$$Q_{\mathrm{i}} = \frac{R^{\mathrm{rad}}}{R^{\mathrm{rad}} + R^{\mathrm{nrad}}}. \tag{4}$$

In Section III and IV we assume for simplicity that the radiative and non-radiative recombination rates show the same voltage dependence, i.e. $R^{\mathrm{rad}}/\, R^{\mathrm{nrad}} = \, R_0^{\mathrm{rad}}/R_0^{\mathrm{nrad}}$. The external surface property, the saturation current densities, are related to the recombination rates as follows

$$J_0 = J_0^{\mathrm{nrad}} + \, J_0^{\mathrm{rad}} = q\int R_0^{\mathrm{nrad}} dx + \, p_{\mathrm{e}}\, q\int R_0^{\mathrm{rad}} dx. \tag{5}$$

Note, that the integral $\int dx$ through the depth of the absorber material connects the non-radiative recombination rate R_0^{nrad} in the thermodynamic equilibrium directly with the non-radiative saturation current J_0^{nrad}, whereas the emission probability p_{e} of the generated photon has to be considered in the case of radiative recombination. As mentioned before, we consider the refractive index to be isotropic and position independent and neglect interference effects. In this approximation, the van Roosbroeck-Shockley equation describes the radiative recombination rate R^{rad} as a function of n, α, and ϕ_{bb} and combined it with equation (2), yields the quantity p_{e}

$$p_{\mathrm{e}} := \frac{J_0^{\mathrm{rad}}/q}{\int R_0^{\mathrm{rad}} dx} = \, \frac{\int A(E)\phi_{\mathrm{bb}}(E)dE}{4\, d\int n^2(E)\, \alpha(E)\phi_{\mathrm{bb}}(E)dE} \tag{6}$$

for non-concentrating solar cells [24]. The emission probability p_{e} is the factor that connects the internal description of a recombination rate R^{rad} to the external description of a current density J_0^{rad}. This factor

depends on the refractive index, i.e. $p_{\mathrm{e}}(n)$. Therefore, we see that we need to consider the refractive index $n(E)$ in addition to the absorption coefficient $\alpha(E)$ for a consistent description of the solar cell behavior from internal to external properties even if the Lambert-Beer Approximation ($A \approx 1 - e^{-2d\alpha}$) is used where $n(E)$ is not needed to calculate the absorptance A. This can intuitively explained by the influence of total internal reflection and subsequent reabsorption ($p_{\mathrm{e}} \leq 1/n^2$) in the absorber material, see Eq. (6).

However, in the widely applied selection metric proposed by Yu and Zunger (spectroscopic limited maximum efficiency – SLME) the refractive index has been neglected. Here an external property, the fraction of radiative electron-hole recombination current $f_{\mathrm{r}} = J_0^{\mathrm{rad}}/J_0$, has been approximated by $f_{\mathrm{r}} = \exp\left((E_{\mathrm{g}} - E_{\mathrm{g}}^{\mathrm{da}})/kT\right)$, where $E_{\mathrm{g}}^{\mathrm{da}}$ is the dipole-allowed transition energy that is calculated by electronic structure theory. Therefore the authors derive external parameters (the ratio of the current densities) from internal parameters (the band gap energy difference $E_{\mathrm{g}} - E_{\mathrm{g}}^{\mathrm{da}}$) without taking the refractive index into account (see Figure S2). This is in contradiction to fundamental laws of physics, given $Q_{\mathrm{i}} \neq 1$, as outlined above. For a more detailed description and discussion of the SLME see Supplemental Material. To show the implications of the negligence of the refractive index we will systematically compare our model to SLME in the following section. For this purpose, we will consider SLME not as a method that determines the efficiency limit for a fixed thickness and a fixed f_{r} given by the band gap differences, but rather as a model that describes a way to calculate the efficiency limit of a device starting from internal material properties. Also, we do not follow the original SLME approach of using the band gap difference as a way of estimating non-radiative recombination. In reality, the non-radiative rate does not just depend on the optical properties of the perfect material, but on the presence of imperfections that act as recombination centers. Therefore, we instead use the internal (luminescence) quantum efficiency Q_{i} as an adjustable parameter, which corresponds to taking f_{r} as an adjustable parameter in the SLME approach.

III. Discussion of models and parameters

The influence of the internal quantum efficiency Q_i, the refractive index n and the thickness d on the efficiency limit is discussed for both models in this section in order to understand the dependencies on these parameters and the resulting difference in the calculated efficiency limits. This systematic study on two exemplarily designed model absorption coefficients in combination with three freely adjustable parameters, e.g. d, Q_i and n, motivates the selection metric that will be introduced in Section IV.

Up to this point, we have learned that we need to know (i.e., compute and/or measure) the absorption coefficient *and* refractive index of a photovoltaic absorber material as *necessary* input for a consistent evaluation of its prospective photovoltaic efficiency limit. Moreover, the step from treating a solar cell in terms of a mere surface with the property of an absorptance towards a material volume related model requires taking the thickness into account. In the first part of this section, we systematically investigate the influence of the cell's thickness on the predicted efficiency potential with the help of model absorption coefficient curves defined by

$$\alpha = \begin{cases} 0 & \text{for } E < E_0 \\ \alpha_0 \exp\left(\frac{E-E_\mathrm{g}}{E_\mathrm{ch}}\right)\sqrt{\frac{E_\mathrm{ch}}{2\exp(1)kT}} & \text{for } E_0 \le E < E_g + \frac{E_\mathrm{ch}}{2} \\ \alpha_0\sqrt{\frac{E-E_\mathrm{g}}{kT}} & \text{for } E \ge E_g + \frac{E_\mathrm{ch}}{2} \end{cases}. \qquad (7)$$

For photon energies $E \geq E_g + \frac{E_\mathrm{ch}}{2}$ the absorption coefficient follows the square root law of a direct semiconductor [64], for $E < E_g + \frac{E_\mathrm{ch}}{2}$ we describe the absorption as an exponential band tail with Urbach energy [65] E_ch and for all energies below the cut-off energy E_0 the absorption is set to zero.

The cut- off energy is motivated by the unavoidable experimental and computational limitations in the determination of α in reality.

Figure 3 depicts the two model absorption coefficients that are used in this work as well as the renowned curve of the SQ efficiency limit over band gap energy E_g (black dashed line). We have chosen one absorption coefficient with a band gap energy of $E_\mathrm{g} = 1.0\ \mathrm{e}V$ and a cut-off energy of $E_0 = 0.9\ \mathrm{e}V$ (red) and another one with $E_\mathrm{g} = 1.5\ \mathrm{e}V$ and $E_0 = 1.4\ \mathrm{e}V$ (blue). The band gap energies as well as the cut-off energies have been selected in a way that they are either both below, or above the two local maxima of the SQ limit. The motivation for this specific choice of energy values becomes clearer in the following discussion of the optimal absorber thickness. The tail slope is in both cases equal to $E_\mathrm{ch} = 0.5\ kT$, a reasonable value for common solar cell materials [66]. The scaling factor α_0 can vary strongly for different materials, but the absolute value is of no importance in the following discussion of our results, as we will only refer to normalized thicknesses $\alpha_0 d$ in this paper. For the sake of simplicity we show the absorption coefficients in Figure 3 exemplarily for $\alpha_0 = 10^5/\mathrm{cm}$.

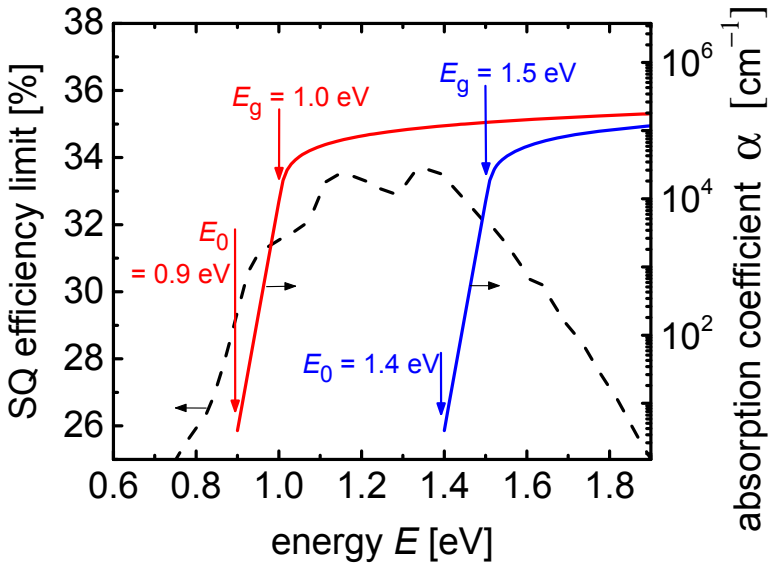

Figure 3: *Two model absorption coefficients versus energy. One absorption coefficient curve (red) is chosen so that both, the band gap energy* $E_\mathrm{g} = 1.0\ \mathrm{eV}$ *and the cut-off energy* $E_0 = 0.9\ \mathrm{eV}$ *are below the maxima of the SQ efficiency limit (black-dashed). The other one (blue) with* $E_\mathrm{g} = 1.5\ \mathrm{eV}$ *and* $E_0 = 1.4\ \mathrm{eV}$ *is only non-zero for energies above* 1.35eV *(second maximum of SQ). In both cases the characteristic energy of the tail is set to* $E_\mathrm{ch} = \frac{1}{2}kT$.

Figure 4a shows the efficiency as a function of normalized thickness $\alpha_0 d$ for these two sample materials in the radiative limit ($Q_\mathrm{i} = 1$) for flat devices. For devices with a Lambertian scatterer as front surface see Figure S3 in the supplemental material. In the case of $E_\mathrm{g} = 1.0\ \mathrm{e}V$ (red), the maximum efficiency is reached at a finite normalized thickness of $\alpha_0 d_\mathrm{opt} \approx 0.7$. In contrast, in the case of $E_\mathrm{g} = 1.5\ \mathrm{e}V$ (blue) the efficiency approaches its maximum at infinite thickness. Monotonic increase in efficiency with thickness for the latter case can be explained by the fact that both E_g and E_0 are above the energy of the maxima of the SQ limit. Making the absorber thicker and thicker leads to an absorption that is closer and closer to a step-like absorption at E_0. As the SQ limit is monotonously decreasing from $1.4\ \mathrm{e}V$ to $1.5\ \mathrm{e}V$ the maximum efficiency for the sample system with $E_\mathrm{g} = 1.5\ \mathrm{e}V$ and $E_0 = 1.4\ \mathrm{e}V$ increases with increasing thickness. The efficiency asymptotically reaches the efficiency of the SQ limit at $1.4\ \mathrm{e}V$, $\eta^\mathrm{SQ}\left(E_\mathrm{g} = 1.4\ eV\right) = \eta^\mathrm{rad}(d = \infty)\big|_{E_0 = 1.4\ eV} \approx 33\ \%$. Following this reasoning, all absorption coefficients with a cut-off energy higher than $1.33\ \mathrm{e}V$, the energy of the second maximum of the SQ limit, reach their maximum efficiency at infinite thickness. The gain in short-circuit current with increasing thickness is in those cases higher than the loss in open-circuit voltage.

The situation is different for band gap energies below the energy of the SQ maxima. For the sample absorption coefficient with $E_\mathrm{g} = 1.0\ \mathrm{e}V$ (red line) the efficiency for infinite thickness is still equal to the

SQ limit of the respective cut-off energy: $\eta^{\mathrm{SQ}}(0.9\,eV) = \eta^{\mathrm{rad}}(d=\infty)\big|_{E_0=0.9\,eV}$. However, this limit $\eta^{SQ}(0.9\,eV)$ is lower than the SQ limit of its corresponding band gap energy $\eta^{SQ}(1.0\ \mathrm{eV})$. Therefore the $\eta^{\mathrm{rad}}(d)$-curve increases until it reaches its maximum of $\eta^{\mathrm{rad}}(d_{\mathrm{opt}}) = 31.17\ \%$, and finally decreases asymptotically towards $\eta^{SQ}(0.9\,eV)$ for infinite thickness. This shows that apparent subtleties of the optical data (namely the cut-off Energy E_0, the photon energy of the first data point with $\alpha > 0$) become quite important when looking for the optimum thickness in the radiative limit.

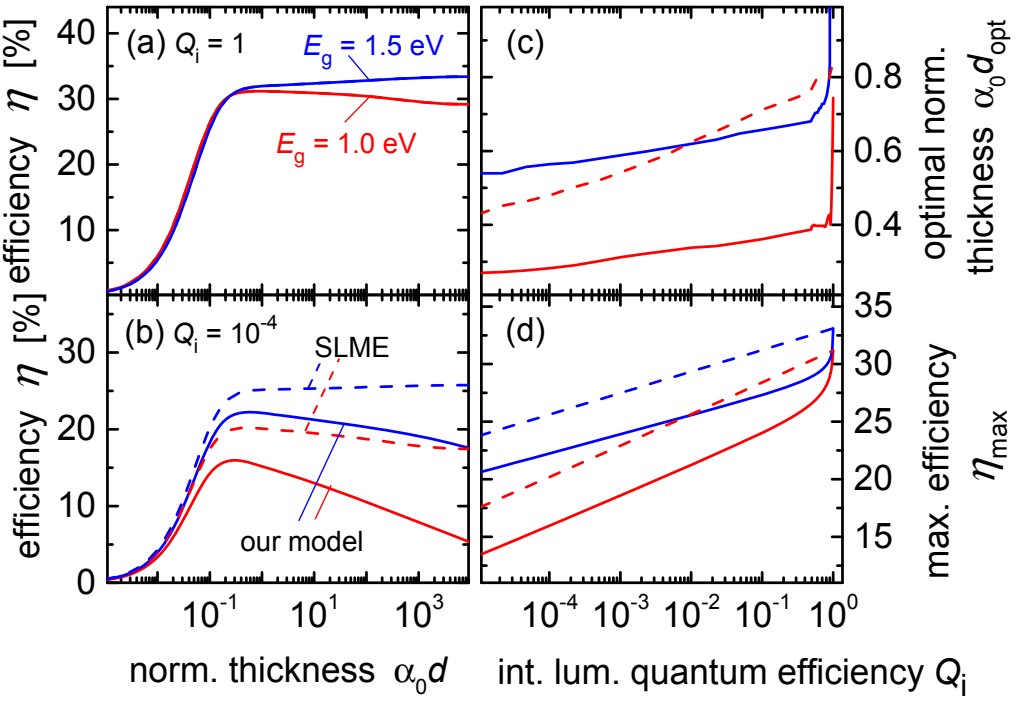

Figure 4: *Efficiency over normalized thickness $\alpha_0 d$ for the model systems $E_{\mathrm{g}} = 1.0$ eV* (red) *and $E_{\mathrm{g}} = 1.5$ eV (blue). The corresponding absorption coefficients are introduced in Fig. 3, the refractive index is set to 3.5. (a) In the radiative limit, $E_{\mathrm{g}} = 1.0$ eV reaches maximum efficiency at an optimal normalized thickness of $\alpha_0 d_{\mathrm{opt}} \approx 0.7$. In contrast, in the case of $E_{\mathrm{g}} = 1.5$ eV the efficiency approaches its maximum at infinite thickness. (b) For $Q_{\mathrm{i}} = 10^{-4}$, the efficiencies as calculated with SLME (dashed lines) and our model (solid lines), which takes the refractive index into account, are seen to deviate from*

one another. The difference in the two models lead to differences in (c) the optimal thickness, for all $Q_\mathrm{i} \neq 1$, as well as (d) the absolute maximal achievable efficiencies η_max, which are significantly overestimated by SLME. Note that in the case of $E_\mathrm{g} = 1.0\ \mathrm{eV}$, the SLME does not predict an optimal thickness, whereas our model always leads to an optimal efficiency for $d \neq \infty$ (given that $Q_\mathrm{i} \neq 1$).

The graph drastically changes when we assume an internal luminescence quantum efficiency of $Q_\mathrm{i} = 10^{-4}$, see Figure 4b. In the case $Q_\mathrm{i} < 1$, the efficiencies calculated from our model (solid lines) and the SLMEs (dashed lines) deviate from one another. In the case for $E_\mathrm{g} = 1.0\ \mathrm{e}V$ (red), both models predict similar optimal thicknesses. The absolute maximum efficiency, however, is with about 20% highly overestimated by SLME in comparison to our model that predicts an efficiency limit of about 16%. Note that in the case of $E_\mathrm{g} = 1.5\ \mathrm{e}V$ (blue) not only the maximum efficiencies deviate strongly, but the curves show a qualitatively different behavior. If one neglects the refractive index (SLME, dashed blue line) the efficiency over thickness curve does not exhibit a global maximum anymore. To explain the observed differences between the two approaches we take a closer look at the equations introduced in Section II.

The short-circuit currents in both models follow directly from $J_\mathrm{sc} = q\int A\phi_\mathrm{sun} dE$ and are therefore independent of Q_i. The saturation current J_0 scales with $1/Q_\mathrm{i}$ in the SLME model, which leads to the same normalized $J_0(d)$-curves for $Q_\mathrm{i} = 1$ and $Q_\mathrm{i} = 10^{-4}$. Therefore J_0 saturates for large thicknesses for all $Q_\mathrm{i} \neq 1$, just like it saturates in the radiative limit. This leads to efficiencies greater than 0% for infinite thickness for all $Q_\mathrm{i} \neq 1$ which is physically unreasonable. In our model on the other hand, the outcoupling efficiency p_e decreases with thickness, which leads to a linear increase in J_0 for sufficiently large thicknesses due to the non-radiative term. Consequently, J_0 does not saturate for $Q_\mathrm{i} < 1$ and our model predicts an efficiency of 0% for infinite thickness, as one would expect.

Figure 4c shows the effect of the internal luminescence quantum efficiency on the optimal normalized thickness. The optimal thicknesses for $E_{\mathrm{g}} = 1.0\ \mathrm{e}V$ (red) and $E_{\mathrm{g}} = 1.5\ \mathrm{e}V$ (blue) are of the same order of magnitude. Same holds for the SLME in the case of $E_{\mathrm{g}} = 1.0\ \mathrm{e}V$ (dashed line). Nevertheless, we would like to point out that the SLME does not predict this strong increase in optimal thickness for the last 10% gain of internal luminescence quantum efficiency ($Q_{\mathrm{i}} = 0.9$ to 1) that is visible in our model (solid lines). As stated above, for the SLME metric the maximum efficiency for $E_{\mathrm{g}} = 1.5\ \mathrm{e}V$ is reached at infinite thickness, and is therefore not present in this graph.

To further analyze the impact of the internal luminescence quantum efficiency and the differences between our model and SLME, we plotted the maximum efficiency at optimal thickness versus the internal luminescence quantum efficiency in Figure 4d. The SLME exhibits a linear decrease in efficiency with decreasing $\ln(Q_{\mathrm{i}})$ for the entire range of Q_{i} shown in this graph. Our model shows the same linear decrease only for $Q_{\mathrm{i}} \ll 1$, whereas we see a dramatic drop in maximum efficiency with decreasing Q_{i} close to the radiative limit of $Q_{\mathrm{i}} = 1$.

As the equations that we use to calculate the maximum efficiency cannot be solved analytically, we use a different approach intuitively explain the observed dependency of the maximum efficiency on Q_{i}. For this purpose we write the efficiency as $\eta = J_{\mathrm{SC}} V_{\mathrm{OC}} FF / P_{\mathrm{sun}}$, where P_{sun} is the power density of the incident sunlight. According to Equation (1), J_{SC} is independent of the internal luminescence quantum efficiency Q_{i}. The fill factor FF can also be considered as being almost independent of the internal luminescence quantum efficiency. Therefore, the derivative of η can be approximately calculated via

$$\frac{d\eta}{d\ln(Q_{\mathrm{i}})} \approx \frac{J_{\mathrm{SC}}\, FF}{P_{\mathrm{sun}}} \cdot \frac{dV_{\mathrm{OC}}}{d\ln(Q_{\mathrm{i}})}. \tag{8}$$

For the SLME metric, J_0 scales with $1/Q_{\mathrm{i}}$ and consequently the open-circuit voltage can be written as $V_{\mathrm{OC}} = V_{\mathrm{OC}}^{\mathrm{rad}} + \frac{kT}{q}\ln(Q_{\mathrm{i}})$, where $V_{\mathrm{OC}}^{\mathrm{rad}}$ is the open-circuit voltage in the radiative limit. With these

considerations we can explain the linear increase in efficiency with $\ln(Q_\mathrm{i})$ for the SLMEs (dashed lines) depicted in Figure 4d.

For $Q_\mathrm{i} = 1$, the SLME limit reaches a value that is between the SQ limit of the band gap energy E_g and the cut-off energy E_0 and is identical to that predicted by our model (solid lines). However, even small deviations in Q_i away from the radiative limit lead to significant differences in the predicted efficiencies. Following Equation (24) in Ref. [24] the open-circuit voltage in our model can be written as

$$V_\mathrm{OC} = V_\mathrm{OC}^\mathrm{rad} + \frac{kT}{q}\ln\left(\frac{p_\mathrm{e}Q_\mathrm{i}}{1 + (p_\mathrm{e}-1)Q_\mathrm{i}}\right), \tag{9}$$

where p_e denotes the probability of a photon that has been generated by radiative recombination to be emitted. Note that we neglect parasitic absorption here as we do throughout our study.

For $Q_\mathrm{i} \ll 1$, the denominator is close to 1 and Equation (9) simplifies to $V_\mathrm{OC} = V_\mathrm{oc}^\mathrm{rad} + \frac{kT}{q}\ln(p_\mathrm{e}Q_\mathrm{i})$ implying the same linear increase in efficiency with $\ln(Q_\mathrm{i})$ as in the SLME, whereas the absolute efficiency is overestimated in the SLME by approximately $\Delta\eta = J_\mathrm{SC}\,FF/P_\mathrm{sun} \cdot \frac{kT}{q}\ln(p_\mathrm{e})$.

For $Q_\mathrm{i} \approx 1$, we cannot neglect the denominator in Equation (9) anymore and the open-circuit voltage, and as a result the efficiency, increase rapidly as Q_i approaches the radiative limit to the same value as predicted by the SLME. Note that the slope in the linear range ($Q_\mathrm{i} \ll 1$) is the same for our model and the SLME. The absolute gradient depends on the band gap energy E_g as we will discuss in the following paragraphs.

Figure 5a shows the maximum efficiency versus internal luminescence quantum efficiency, just like Figure 4d, but for various band gap energies and calculated by our model only. Here we assume again flat surfaces (for the case of a Lambertian scatterer as front surface see Figure S4 in the Supplemental Material). All absorption coefficients used are defined by Equation (7) with $E_\mathrm{g} = 0.7$ to 1.9 eV in steps

of $0.2\ \mathrm{e}V$ (red to blue, (i) to (viii)), the characteristic energy is $E_{\mathrm{ch}} = 0.5\ kT$ and the cut-off energies are $0.1\ \mathrm{e}V$ below the respective band gap energies, $E_0 = E_{\mathrm{g}} - 0.1\ \mathrm{eV}$. The maximum efficiency in the radiative limit is reached for band gaps of $1.3\ \mathrm{e}V$ and $1.5\ \mathrm{e}V$ with cut-off energies of $1.2\ \mathrm{e}V$ and $1.4\ \mathrm{e}V$ respectively. This is expected given the band gap energies of the SQ efficiency maxima plotted in Figure 3. All curves show the already discussed significant drop in efficiency as Q_{i} decreases from 100% to 60%. For all $Q_{\mathrm{i}} < 60\%$, the efficiency decreases linearly with decreasing $\ln(Q_{\mathrm{i}})$ until it asymptotically approaches 0 %, as can be surmised for very low Q_{i} in the case of $E_{\mathrm{g}} = 0.7\ \mathrm{e}V$ (red line).

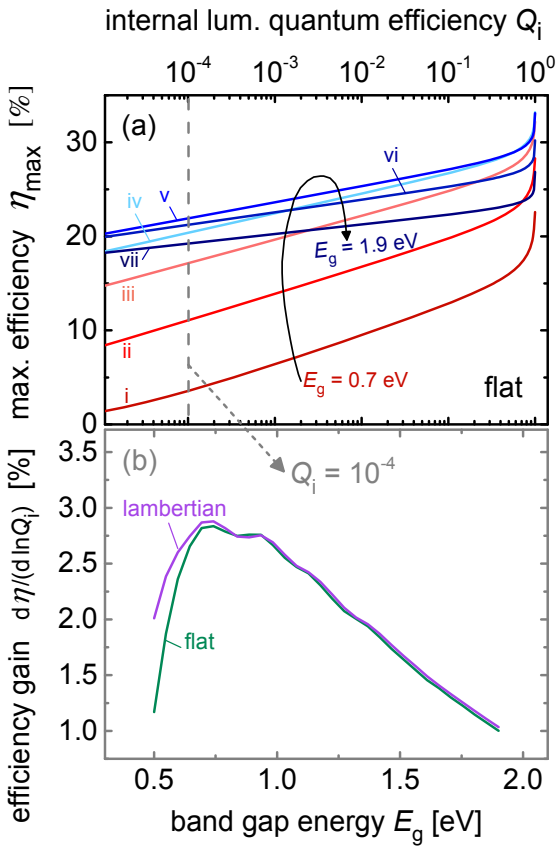

Figure 5: *(a) Maximum efficiency versus internal quantum efficiency* Q_{i} *for band gaps* $E_{\mathrm{g}} = 0.7$ *to* 1.9 eV *in steps of* 0.2 eV *(red to blue,* (i) *to* (vii)*) assuming flat devices. Note how both, the absolute efficiency*

for $Q_\mathrm{i} = 1$ and the slope of the efficiency, depend on E_g. (b) The derivative $d\eta/d\ln(Q_\mathrm{i})$ plotted as a function of E_g for flat surfaces (green) and Lambertian scatterers (purple) at $Q_\mathrm{i} = 10^{-4}$.

We concentrate now on the linear slope of $\eta(\ln Q_\mathrm{i})$. Figure 5b presents the derivative $\frac{d\eta}{d\ln(Q_\mathrm{i})}$ as a function of band gap energy for $Q_\mathrm{i} = 10^{-4}$. This function is almost independent of the assumed light-trapping scheme [62]. A Lambertian light scatterer as front surface (purple) only slightly deviates from a flat front surface (green) for very low band gaps $E_\mathrm{g} < 0.7\ \mathrm{e}V$. For band gap energies above $0.7\ \mathrm{e}V$, the gain in efficiency $\frac{d\eta}{d\ln(Q_\mathrm{i})}$, is monotonically decreasing from 3% to 1% absolute efficiency per decade of internal luminescence quantum efficiency. As the gain in efficiency can be expressed by $\frac{d\eta}{d\ln(Q_\mathrm{i})}(E_\mathrm{g}) \approx J_\mathrm{SC}(E_\mathrm{g})\, FF(E_\mathrm{g})\, \frac{kT}{q\, P_\mathrm{sun}}$, the shape of the curve $\frac{d\eta}{d\ln(Q_\mathrm{i})}$ plotted in Figure 5b, can be explained by the dependency of the product $FF \cdot J_\mathrm{SC}$ on the band gap energy E_g. Whereas J_SC decreases monotonously with band gap, the fill factor increases strongly for small band gaps and saturates for higher band gap energies, the product of these two curves result in the curve of the efficiency gain $\frac{d\eta}{d\ln(Q_\mathrm{i})}$ as illustrated in Figure 5b.

After discussing the impact of the internal luminescence quantum efficiency and the thickness on the maximum efficiency, we want to close this section with analyzing the effect of the refractive index on the maximal achievable efficiency. For simplicity we will only discuss this for the case $E_\mathrm{g} = 1.5\ \mathrm{e}V$, the analogous graph for $E_\mathrm{g} = 1.0\ \mathrm{e}V$ is displayed in Figure S5 in the supplemental material.

Figure 6 illustrates the dependency of the efficiency limit on the refractive index calculated by our model and the SLME model. For $Q_\mathrm{i} = 1$ (solid line), there is no difference between our model and the SLME as has been pointed out. The maximum efficiency in the radiative limit is approximately 33.4%

independent of the light-trapping scheme, see Figure 6a for a flat front surface and Figure 6b for a Lambertian scatterer as front surface. The value reached is equal to the SQ limit for $E_{\mathrm{g}} = 1.4\ \mathrm{e}V$ which corresponds to the cut-off energy $E_0 = 1.4\ \mathrm{e}V$ of the examined absorption coefficient. In the SLME the achievable efficiency is independent of the refractive index and the texture of the front surface independent of Q_{i}. In contrast, our model (dash-dotted line) shows a relative decrease in efficiency of 20% as the refractive index varies from 1 to 10 for flat surfaces. Therefore the overestimation of the maximum efficiency by SLME increases with increasing refractive index.

The decrease in efficiency with refractive index in our model is a direct consequence of Equation (6). The radiative recombination rate R^{rad} is proportional to n^2, and because we hold $Q_{\mathrm{i}} = 10^{-4}$ constant the non-radiative recombination rate R^{nrad} has to have the same dependence on n as R^{rad} according to Equation (4). Note that $Q_{\mathrm{i}} = 10^{-4}$ implies $R^{\mathrm{rad}} \ll R^{\mathrm{nrad}}$. Consequently, the saturation current J_0 inreases with n^2 and the efficiency η decreases linearly with $\ln(n)$, as seen in Figure 6a in the case of flat devices. For devices with a Lambertian scatterer as front surface the absorption $A(E)$ and therefore the short-circuit current J_{SC} are increasing with n. This increase in J_{SC} compensates the increase of J_0 to some extent and the loss in efficiency with n for fixed $Q_{\mathrm{i}} = 10^{-4}$ is smaller, see dashed-dotted line in Figure 6b.

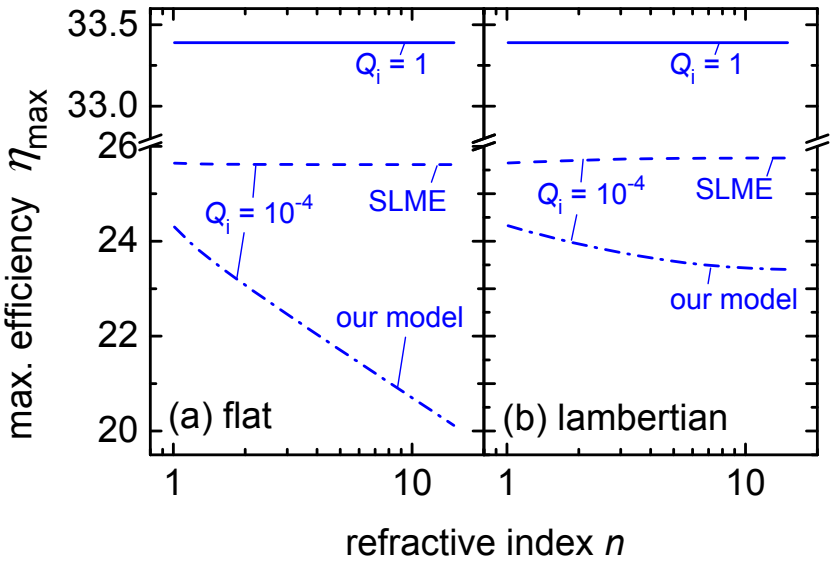

Figure 6: *Dependence of the maximum efficiency $\eta_{\max}$ on the refractive index n for $E_g = 1.5$ eV. In both, the radiative limit ($Q_i = 1$, solid lines) and the SLME for $Q_i = 10^{-4}$ (dashed lines), the efficiencies are independent of n. (a) On the other hand our model (dashed-dotted line) shows a significant efficiency drop of almost 20% as the refractive index n varies from 1 to 10 for flat devices. (b) Assuming a Lambertian scatterer, the refractive index has a much weaker influence of a mere 4%.*

IV. Recipe to calculate efficiency limits

After the detailed discussion of different models and their behavior under certain circumstances we achieved a deeper understanding of how to calculate a reasonable and also practical efficiency limit from available optical data, either gathered by experiments or from electronic structure calculations. Given the strong dependence of the maximum efficiency on the refractive index, we conclude that the real part of the refractive index must not be neglected. Moreover, the calculated efficiency is also very sensitive on the internal luminescence quantum efficiency, see Figure 5. The internal luminescence

quantum efficiency Q_i is a complex interplay between energy levels in the material, defects, and kinetics in the device. It is therefore very challenging to determine Q_i computationally but it might be possible to determine it experimentally without having to fabricate devices [57]. Approaches for first-principles calculations of non-radiative recombination rates due to point defects are emerging [67-69] and could provide in the future at least an estimate of the upper limit of Q_i under idealized situations. In practice, it is useful to treat the internal luminescence quantum efficiency as an independent parameter, in particular at an early stage of material investigation when materials growth and device fabrication have not yet been optimized. A third point that we want to stress is the thickness dependency of the efficiency. Our results presented in Section III show that a comparison of different materials at a fixed thickness favor certain materials over others without proper justification. Therefore the optimal thickness should be considered in the figure of merit for all cases with $Q_\mathrm{i} < 1$.

We propose to make full use of the available optical data from electronic structure theory to estimate the potential of a new material as follows: 1. Decide on a light trapping scheme to calculate the absorptance A from the absorption coefficienct α, e.g. for flat devices use Equation (S1) in the supplemental material. 2. Calculate the short-circuit current J_SC, and the radiative saturation current J_0^rad according to Equations (1) and (2) which leads to the radiative efficiency limit via Equation (3). 3. Calculate the absorbance and efficiency for numerous thicknesses to end up with an efficiency-over-thickness curve $\eta(d)$. 4. Find the maximum of this curve $\max\left(\eta(d)\right) = \eta(d_\mathrm{opt})$ and the corresponding optimal thickness d_opt. 5. For reasons stated above we suggest to repeat steps 1-3 for a number of reasonable internal luminescence quantum efficiencies. Note, that for $Q_\mathrm{i} \neq 1$, we need in addition to Equations (1)-(3) Equations (4)-(6) to determine the efficiency limit. Additionally, we would like to point out that this selection metric just like the selection metric from Yu and Zunger can only be applied to materials with a tail slope E_ch smaller than kT, see Supplemental Material.

Exemplarily we apply the suggested method to a few complex refractive indices that have been determined via first principles calculations. These calculations were performed within the GW approximation [55], as implemented in the VASP code [70, 71], and are part of a larger database (http://materials.nrel.gov). A more detailed description of the approach is given in Ref. [72, 73]. For this dataset, the dielectric function is calculated in the independent particle approximation. Figure 7 presents the input data in the form of absorption coefficients α and the refractive index n as a function of photon energy E. We applied the method exemplarily to eight materials, namely $CuInSe_2$ (grey), $Cu_2ZnSnSe_4$ (CZTSe - red), $CuSbSe_2$ (orange), Sb_2Se_3 (green), CZTS (turquoise), $CuGaSe_2$ (blue), $CuSbS_2$ (purple) and Sb_2S_3 (pink). All these materials have sharp absorption edges with $E_{\mathrm{ch}} < kT$, a reasonable absorption coefficient for high energies between 10^5 – 10^6 /cm, and band gap energies between 1 and 2 $\mathrm{e}V$. So at first sight they are all promising photovoltaic absorber materials.

Figure 8 illustrates the maximum efficiencies calculated according to our method for internal luminescence quantum efficiencies $\log(Q_{\mathrm{i}}) = 0$ to -7 in steps of -1 (dark to light) sorted by the energy of the direct band gap. In the radiative limit ($Q_{\mathrm{i}} = 1$) the highest efficiencies are reached for CZTSe (red), $CuSbSe_2$ (orange), and Sb_2Se_3 (green). This corresponds well with the maxima of the SQ limit as depicted in Figure 3 at the beginning of Section III, which predicts the highest efficiencies for materials with band gap energies of $1.1 - 1.3\ \mathrm{e}V$. Assuming more realistic quantum efficiencies of $Q_{\mathrm{i}} < 10^{-2}$, the highest efficiency is reached for CZTS with a band gap energy of approximately $1.56\ \mathrm{e}V$. This is a direct

consequence of the band gap dependent loss in efficiency due to the internal luminescence quantum efficiency. This effect has been addressed in detail in the scope of Figure 5. Note, that all these efficiencies have been calculated assuming flat devices, with a perfect back reflector and no reflectivity at the front surface.

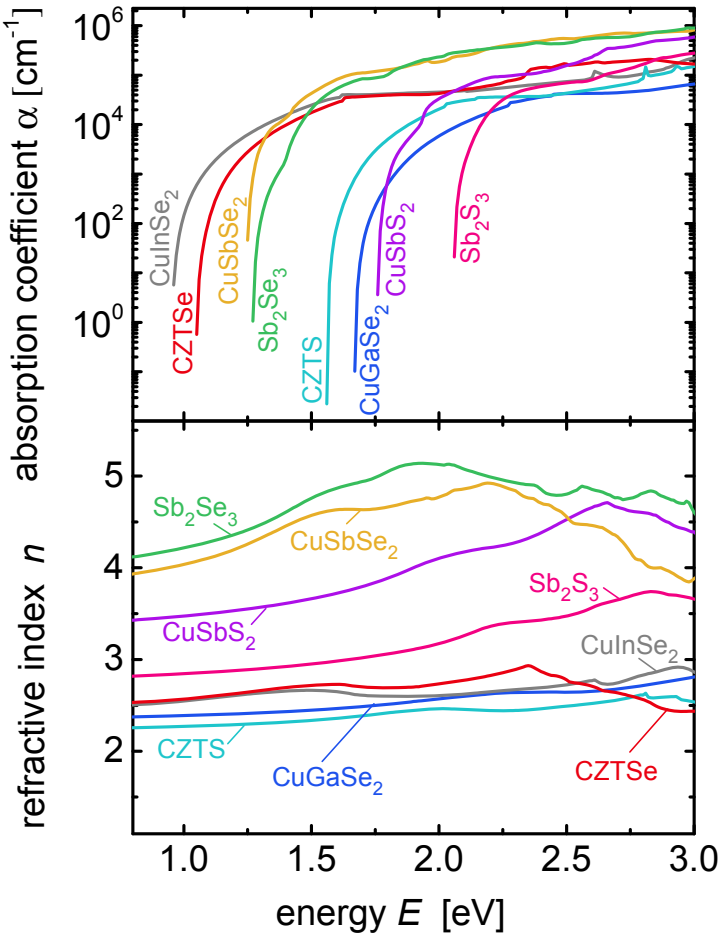

Figure 7: *Absorption coefficient α and refractive index n of $CuInSe_2$ (grey), CZTSe (red), $CuSbSe_2$ (orange), Sb_2Se_3 (green), CZTS (turquoise), $CuGaSe_2$ (blue), $CuSbS_2$ (purple), Sb_2S_3 (pink) as a function of energy as simulated via electronic structure theory.*

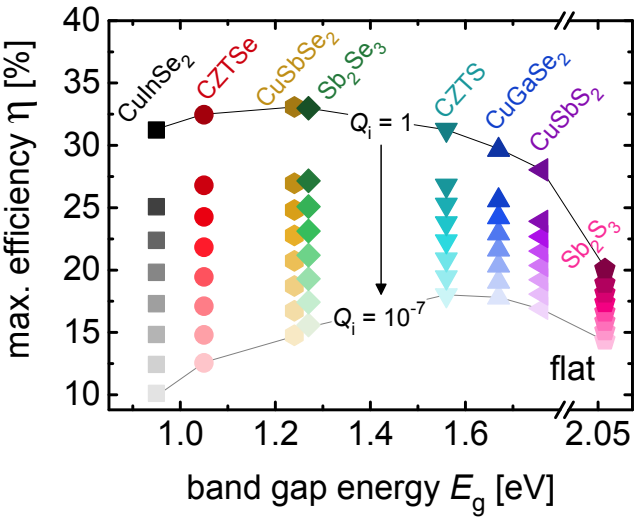

Figure 8: *Maximal efficiencies of 8 materials (sorted by direct band gap, see Figure 6) for different internal quantum efficiencies* $log(Q_i) = 0$ *to -7 in steps of -1 (dark to light colors). For* $Q_i = 1$*,* $CuSbSe_2$ *achieves the highest efficiency, whereas for* $Q_i < 10^{-2}$ *CZTS takes the lead.*

However, these results are not very conclusive yet:: For instance in the radiative limit, a very weakly absorbing material could outperform other materials with higher absorption if one does not consider the thickness of the device. As the non-radiative recombination in the bulk can normally not be neglected, the carrier collection efficiency decreases significantly with thickness. Additionally very thick devices will in real life exhibit very low efficiencies due to the finite mobility of the investigated materials. Therefore in a realistic scenario, we aim for a material that can reach as high efficiencies as possible at as small a thickness as possible.

In Figure 9 we plotted the maximum efficiency over the optimal thickness d_{opt} for the same 8 materials (colors and symbols analogously to Figure 8) to address the importance of thickness to a selection metric. In this case we excluded the case $Q_i = 1$, as some of the samples reach their efficiency maximum at infinite thickness for $Q_i = 1$, which is unreasonable for a realistic estimation of the

photovoltaic potential of a certain material. For flat surfaces as shown in Figure 9a $CuSbSe_2$ (orange) exhibits the smallest optimal thicknesses between 600 nm for $Q_\mathrm{i} = 10^{-7}$ and 1 µm for $Q_\mathrm{i} = 0.1$. In Figure 9b we assumed a Lambertian scatterer as front surface and a perfect flat back reflector. This light-trapping scheme leads to considerably smaller optimal thicknesses and higher efficiencies for all materials. The quantitative gain in efficiency and loss in optimal thickness is however distinct for each material. This becomes apparent when looking at the difference in optimal thickness between $CuInSe_2$ (grey), and $CuSbS_2$ (purple). For flat devices the optimal thicknesses for $CuInSe_2$ are on average 5 µm smaller than for $CuSbS_2$. On the other hand, assuming a Lambertian light scatterer this difference in optimal thickness diminishes, e.g. $d_\mathrm{opt}(CuSbS_2) < d_\mathrm{opt}(CuInSe_2)$ for high Q_i and $d_\mathrm{opt}(CuSbS_2) > d_\mathrm{opt}(CuInSe_2)$ for low Q_i. Given this analysis we conclude that $CuSbSe_2$ reaches the highest efficiencies for the smallest thicknesses and therefore is an excellent candidate for a high performing photovoltaic absorber material based on its complex refractive index.

Given that the materials presented in Figures 6 to 8 are all materials that have already been used for photovoltaics, it is worth briefly comparing the results of our assessment based on complex refractive index and internal luminescence quantum efficiency with the empirical results for these technologies. While a technology like $Cu(In,Ga)Se_2$ is capable of achieving efficiencies > 22%,[74] our analysis for a at constant Q_i would not state that this material would be superior to the others just based on its complex refractive index. This is not particularly surprising given that our selection of materials generally exhibit quite good optical properties for photovoltaic applications. The current lack of success of materials such as CZTSe [75], $CuSbS_2$ [76, 77] or $CuSbSe_2$ [78] is a matter of Q_i being lower than for $Cu(In,Ga)Se_2$. Thus, there is a need for computational materials screening to focus on parameters that are related to the presence of defects such as the search for defect-tolerant materials.

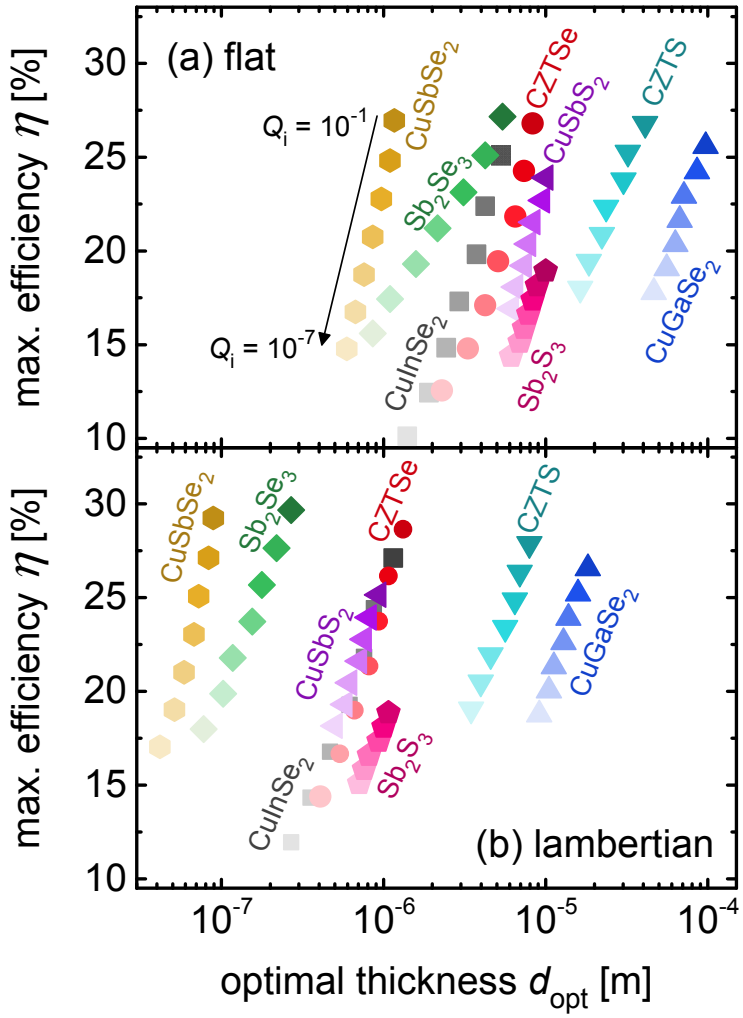

Figure 9: *Efficiency at the optimal thickness for the same materials (see Fig. 7) for internal quantum efficiencies* $\log(Q_i)$ *=-1, -2, -3, -4, -5, -6, -7 (colors and symbols same as in Fig. 8) with (a) a flat front surface and (b) a Lambertian scatterer as front surface. For both systems a perfect flat mirror as back reflector is assumed.*

V. Conclusions and Outlook

The present paper has shown that for successful computational screening of prospective photovoltaic materials a thermodynamically correct translation of material data into photovoltaic output data is mandatory. For this purpose, we have defined a hierarchy of extension steps (see Figure 1) that allows gradually to add physical specifications to the original SQ approach. The first, *impartible* step towards more detail than the band gap energy embraces knowledge of the complex refractive index of photovoltaic absorber materials as a *necessary* input parameter. As this step deduces the absorptance from the absorption coefficient, asumptions on device thickness and light trapping scheme must also be made. The choice of a Lambertian light trapping scheme as the reference case seems appropriate due to its physical simplicity and practical relevance. The obvious choice for device thickness is then the one that yields the highest efficiency.

The second step towards more detail is the introduction of non-radiative recombination, i.e., the departure from an internal luminescence quantum efficiency $Q_i = 1$. This step necessarily implies that step 1 has been conducted correctly. Failure to do so implies misinterpretation of material data, for instance by neglecting that internal and external quantum efficiency differ significantly. The present paper restricts itself to the demonstration of steps 1 and 2. However, the next level of detailing obviously would be the departure from virtually infinite mobility. –in this case additional assumptions on junction type and doping densities are necessary [53, 79]. It is important to notice that the level of sophistication of such models is still far below that of a specific device model. We are still dealing with generic models and a very low level of computational effort compared to that needed to provide the initial first principle data.

In view of computational materials screening, the positive message is that the data that are necessary for the first step of detailing are also most easily obtained numerically. However, this does not imply that these properties (absorption coefficient and refractive index) are the most decisive ones. In view of the fact that most practical photovoltaic devices and even most record devices are limited by non-radiative recombination [80, 81], urges us to get access to this loss mechanism by first principle calculations. For instance the tendency of some types of semiconductors to build shallow instead of deep intrinsic defects [82, 83] is certainly an important hint towards prospective photovoltaic performance. Therefore, extending the scope of high-throughput computations to more detailed properties by carefully stepping down the abstraction pyramide (see Figure 1) will have a high impact on successful selection and implementation of novel PV materials.

Acknowledgement

The authors thank Urs Aeberhard for a helpful and critical discussion of the manuscript. We acknowledge support from the DFG (Grant Nos. KI-1571/2-1 and RA 473/7-1) and from the Helmholtz Foundation via the Helmholtz-NREL Solar Energy Initiative. BB thanks the Bosch-Forschungsstiftung for a PhD scholarship. SL was supported by the US Department of Energy, Office of Science, Basic Energy Sciences, as part of an Energy Frontier Research Center, under contract DE-AC36-08GO28308 to NREL.

References

[1] W. F. Maier, K. Stowe, and S. Sieg, "Combinatorial and high-throughput materials science", Angew Chem Int Edit **46**, 6016 (2007).

[2] S. Curtarolo, G. L. W. Hart, M. B. Nardelli, N. Mingo, S. Sanvito, and O. Levy, "The high-throughput highway to computational materials design", Nat Mater **12**, 191 (2013).

[3] A. Jain, S. P. Ong, G. Hautier, W. Chen *et al.*, "Commentary: The Materials Project: A materials genome approach to accelerating materials innovation", Apl Mater **1**, 011002 (2013).

[4] J. Hachmann, R. Olivares-Amaya, A. Jinich, A. L. Appleton *et al.*, "Lead candidates for high-performance organic photovoltaics from high-throughput quantum chemistry - the Harvard Clean Energy Project", Energy & Environmental Science **7**, 698 (2014).

[5] C. Wadia, A. P. Alivisatos, and D. M. Kammen, "Materials Availability Expands the Opportunity for Large-Scale Photovoltaics Deployment", Environmental Science & Technology **43**, 2072 (2009).

[6] R. E. Brandt, V. Stevanović, D. S. Ginley, and T. Buonassisi, "Identifying defect-tolerant semiconductors with high minority-carrier lifetimes: beyond hybrid lead halide perovskites", MRS Communications **5**, 265 (2015).

[7] I. E. Castelli, T. Olsen, S. Datta, D. D. Landis, S. Dahl, K. S. Thygesen, and K. W. Jacobsen, "Computational screening of perovskite metal oxides for optimal solar light capture", Energy & Environmental Science **5**, 5814 (2012).

[8] A. J. Lehner, D. H. Fabini, H. A. Evans, C.-A. Hébert, S. R. Smock, J. Hu, H. Wang, J. W. Zwanziger, M. L. Chabinyc, and R. Seshadri, "Crystal and Electronic Structures of Complex Bismuth Iodides A3Bi2I9 (A = K, Rb, Cs) Related to Perovskite: Aiding the Rational Design of Photovoltaics", Chemistry of Materials **27**, 7137 (2015).

[9] R. X. Yang, K. T. Butler, and A. Walsh, "Assessment of Hybrid Organic–Inorganic Antimony Sulfides for Earth-Abundant Photovoltaic Applications", The Journal of Physical Chemistry Letters **6**, 5009 (2015).

[10] A. M. Ganose, K. T. Butler, A. Walsh, and D. O. Scanlon, "Relativistic electronic structure and band alignment of BiSI and BiSeI: candidate photovoltaic materials", J Mater Chem A **4**, 2060 (2016).

[11] M. R. Filip, and F. Giustino, "Computational Screening of Homovalent Lead Substitution in Organic–Inorganic Halide Perovskites", The Journal of Physical Chemistry C **120**, 166 (2016).

[12] K. T. Butler, J. M. Frost, J. M. Skelton, K. L. Svane, and A. Walsh, "Computational materials design of crystalline solids", Chemical Society Reviews **45**, 6138 (2016).

[13] N. M. O'Boyle, C. M. Campbell, and G. R. Hutchison, "Computational Design and Selection of Optimal Organic Photovoltaic Materials", The Journal of Physical Chemistry C **115**, 16200 (2011).

[14] A. Yosipof, O. E. Nahum, A. Y. Anderson, H.-N. Barad, A. Zaban, and H. Senderowitz, "Data Mining and Machine Learning Tools for Combinatorial Material Science of All-Oxide Photovoltaic Cells", Molecular Informatics **34**, 367 (2015).

[15] W. Shockley, and H. J. Queisser, "Detailed Balance Limit of Efficiency of P-N Junction Solar Cells", J Appl Phys **32**, 510 (1961).

[16] J. Mattheis, J. H. Werner, and U. Rau, "Finite mobility effects on the radiative efficiency limit of pn-junction solar cells", Phys Rev B **77**, 085203 (2008).

[17] T. Kirchartz, J. Mattheis, and U. Rau, "Detailed balance theory of excitonic and bulk heterojunction solar cells", Phys Rev B **78**, 235320 (2008).

[18] T. Tiedje, E. Yablonovitch, G. D. Cody, and B. G. Brooks, "Limiting efficiency of silicon solar cells", IEEE Transactions on Electron Devices **31**, 711 (1984).

[19] M. A. Green, "Limits on the open-circuit voltage and efficiency of silicon solar cells imposed by intrinsic Auger processes", IEEE Transactions on Electron Devices **31**, 671 (1984).

[20] T. Kirchartz, F. Staub, and U. Rau, "Impact of Photon Recycling on the Open-Circuit Voltage of Metal Halide Perovskite Solar Cells", ACS Energy Letters **1**, 731 (2016).
[21] R. T. Ross, "Some Thermodynamics of Photochemical Systems", J Chem Phys **46**, 4590 (1967).
[22] U. Rau, "Reciprocity relation between photovoltaic quantum efficiency and electroluminescent emission of solar cells", Phys Rev B **76**, 085303 (2007).
[23] M. A. Green, "Radiative efficiency of state-of-the-art photovoltaic cells", Progress in Photovoltaics: Research and Applications **20**, 472 (2012).
[24] U. Rau, U. W. Paetzold, and T. Kirchartz, "Thermodynamics of light management in photovoltaic devices", Phys Rev B **90**, 035211 (2014).
[25] K. Vandewal, K. Tvingstedt, A. Gadisa, O. Inganas, and J. V. Manca, "On the origin of the open-circuit voltage of polymer-fullerene solar cells", Nat Mater **8**, 904 (2009).
[26] J. Yao, T. Kirchartz, M. S. Vezie, M. A. Faist *et al.*, "Quantifying Losses in Open-Circuit Voltage in Solution-Processable Solar Cells", Physical Review Applied **4**, 014020 (2015).
[27] C.-H. M. Chuang, A. Maurano, R. E. Brandt, G. W. Hwang, J. Jean, T. Buonassisi, V. Bulović, and M. G. Bawendi, "Open-Circuit Voltage Deficit, Radiative Sub-Bandgap States, and Prospects in Quantum Dot Solar Cells", Nano Letters **15**, 3286 (2015).
[28] B. Minnaert, and M. Burgelman, "Efficiency potential of organic bulk heterojunction solar cells", Prog Photovoltaics **15**, 741 (2007).
[29] H. J. Snaith, "Estimating the Maximum Attainable Efficiency in Dye-Sensitized Solar Cells", Adv Funct Mater **20**, 13 (2010).
[30] U. Rau, F. Einsele, and G. C. Glaeser, "Efficiency limits of photovoltaic fluorescent collectors", Appl Phys Lett **87**, 171101 (2005).
[31] L. J. A. Koster, S. E. Shaheen, and J. C. Hummelen, "Pathways to a New Efficiency Regime for Organic Solar Cells", Adv Energy Mater **2**, 1246 (2012).
[32] U. Rau, and J. H. Werner, "Radiative efficiency limits of solar cells with lateral band-gap fluctuations", Appl Phys Lett **84**, 3735 (2004).
[33] T. Kirchartz, K. Taretto, and U. Rau, "Efficiency Limits of Organic Bulk Heterojunction Solar Cells", The Journal of Physical Chemistry C **113**, 17958 (2009).
[34] M. J. Kerr, A. Cuevas, and P. Campbell, "Limiting efficiency of crystalline silicon solar cells enhanced to Coulomb-enhanced auger recombination", Prog Photovoltaics **11**, 97 (2003).
[35] O. D. Miller, E. Yablonovitch, and S. R. Kurtz, "Strong Internal and External Luminescence as Solar Cells Approach the Shockley-Queisser Limit", IEEE Journal of Photovoltaics **2**, 303 (2012).
[36] M. A. Steiner, J. F. Geisz, I. Garcia, D. J. Friedman, A. Duda, and S. R. Kurtz, "Optical enhancement of the open-circuit voltage in high quality GaAs solar cells", J Appl Phys **113**, 123109 (2013).
[37] L. P. Yu, and A. Zunger, "Identification of Potential Photovoltaic Absorbers Based on First-Principles Spectroscopic Screening of Materials", Phys Rev Lett **108**, 068701 (2012).
[38] C. N. Savory, A. Walsh, and D. O. Scanlon, "Can Pb-Free Halide Double Perovskites Support High-Efficiency Solar Cells?", ACS Energy Letters, 949 (2016).
[39] A. Zakutayev, X. W. Zhang, A. Nagaraja, L. P. Yu, S. Lany, T. O. Mason, D. S. Ginley, and A. Zunger, "Theoretical Prediction and Experimental Realization of New Stable Inorganic Materials Using the Inverse Design Approach", J Am Chem Soc **135**, 10048 (2013).
[40] L. P. Yu, R. S. Kokenyesi, D. A. Keszler, and A. Zunger, "Inverse Design of High Absorption Thin-Film Photovoltaic Materials", Adv Energy Mater **3**, 43 (2013).
[41] C. N. Savory, A. M. Ganose, W. Travis, R. S. Atri, R. G. Palgrave, and D. O. Scanlon, "An assessment of silver copper sulfides for photovoltaic applications: theoretical and experimental insights", J Mater Chem A **4**, 12648 (2016).

[42] T. Yokoyama, F. Oba, A. Seko, H. Hayashi, Y. Nose, and I. Tanaka, "Theoretical Photovoltaic Conversion Efficiencies of ZnSnP2, CdSnP2, and Zn1-xCdxSnP2 Alloys", Appl Phys Express **6**, 061201 (2013).
[43] I.-H. Lee, J. Lee, Y. J. Oh, S. Kim, and K. Chang, "Computational search for direct band gap silicon crystals", Phys Rev B **90**, 115209 (2014).
[44] Y. J. Oh, I.-H. Lee, S. Kim, J. Lee, and K. J. Chang, "Dipole-allowed direct band gap silicon superlattices", Sci Rep-Uk **5**, 18086 (2015).
[45] W.-J. Yin, T. Shi, and Y. Yan, "Superior Photovoltaic Properties of Lead Halide Perovskites: Insights from First-Principles Theory", The Journal of Physical Chemistry C **119**, 5253 (2015).
[46] M. Bercx, N. Sarmadian, R. Saniz, B. Partoens, and D. Lamoen, "First-principles analysis of the spectroscopic limited maximum efficiency of photovoltaic absorber layers for CuAu-like chalcogenides and silicon", Phys Chem Chem Phys **18**, 20542 (2016).
[47] W. Meng, B. Saparov, F. Hong, J. Wang, D. B. Mitzi, and Y. Yan, "Alloying and Defect Control within Chalcogenide Perovskites for Optimized Photovoltaic Application", Chemistry of Materials **28**, 821 (2016).
[48] N. Sarmadian, R. Saniz, B. Partoens, and D. Lamoen, "First-principles study of the optoelectronic properties and photovoltaic absorber layer efficiency of Cu-based chalcogenides", J Appl Phys **120**, 085707 (2016).
[49] J. Heo, R. Ravichandran, C. F. Reidy, J. Tate, J. F. Wager, and D. A. Keszler, "Design Meets Nature: Tetrahedrite Solar Absorbers", Adv Energy Mater **5**, 1401506 (2015).
[50] R. Brendel, and R. Peibst, "Contact Selectivity and Efficiency in Crystalline Silicon Photovoltaics", Ieee J Photovolt **6**, 1413 (2016).
[51] T. Tiedje, E. Yablonovitch, G. D. Cody, and B. G. Brooks, "Limiting Efficiency of Silicon Solar-Cells", IEEE Trans.Elec.Dev. **31**, 711 (1984).
[52] A. Marti, J. L. Balenzategui, and R. F. Reyna, "Photon recycling and Shockley's diode equation", Journal of Applied Physics **82**, 4067 (1997).
[53] J. Mattheis, J. H. Werner, and U. Rau, "Finite mobility effects on the radiative efficiency limit of pn-junction solar cells", Phys.Rev.B **77**, 085203 (2008).
[54] T. Kirchartz, and U. Rau, "Decreasing Radiative Recombination Coefficients via an Indirect Band Gap in Lead Halide Perovskites", J Phys Chem Lett **8**, 1265 (2017).
[55] L. Hedin, "New Method for Calculating 1-Particle Greens Function with Application to Electron-Gas Problem", Phys Rev **139**, A796 (1965).
[56] A. Richter, M. Hermle, and S. W. Glunz, "Reassessment of the Limiting Efficiency for Crystalline Silicon Solar Cells", IEEE Journal of Photovoltaics **3**, 1184 (2013).
[57] F. Staub, H. Hempel, J.-C. Hebig, J. Mock, U. W. Paetzold, U. Rau, T. Unold, and T. Kirchartz, "Beyond Bulk Lifetimes: Insights into Lead Halide Perovskite Films from Time-Resolved Photoluminescence", Physical Review Applied **6**, 044017 (2016).
[58] A. International, (ASTM International, West Conshohocken, PA, 2012).
[59] Alternatively one could explain the perfect charge carrier collection by an infinite charge carrier mobility combined with a *finite* thickness. However, this still leads to contradiction assumptions as the device has to be infinitely thick for the step-like absorption.
[60] U. Aeberhard, "Quantum-kinetic theory of steady-state photocurrent generation in thin films: Coherent versus incoherent coupling", Phys Rev B **89**, 115303 (2014).
[61] U. Aeberhard, and U. Rau, "Microscopic Perspective on Photovoltaic Reciprocity in Ultrathin Solar Cells", Physical Review Letters **118**, 247702 (2017).
[62] See Supplemental Material at [URL will be inserted by publisher] for a more detailed explanation on the light-trapping schemes.

[63] M. A. Green, "Lambertian light trapping in textured solar cells and light-emitting diodes: Analytical solutions", Prog Photovoltaics **10**, 235 (2002).
[64] S. M. Sze, *Physics of Semiconductor Devices* (John Wiley & Sons, New York, 1936).
[65] F. Urbach, "The Long-Wavelength Edge of Photographic Sensitivity and of the Electronic Absorption of Solids", Phys Rev **92**, 1324 (1953).
[66] S. De Wolf, J. Holovsky, S.-J. Moon, P. Löper, B. Niesen, M. Ledinsky, F.-J. Haug, J.-H. Yum, and C. Ballif, "Organometallic Halide Perovskites: Sharp Optical Absorption Edge and Its Relation to Photovoltaic Performance", The Journal of Physical Chemistry Letters **5**, 1035 (2014).
[67] A. Alkauskas, Q. Yan, and C. G. Van de Walle, "First-principles theory of nonradiative carrier capture via multiphonon emission", Phys Rev B **90**, 075202 (2014).
[68] L. Shi, K. Xu, and L.-W. Wang, "Comparative study of ab initio nonradiative recombination rate calculations under different formalisms", Phys Rev B **91**, 205315 (2015).
[69] G. D. Barmparis, Y. S. Puzyrev, X. G. Zhang, and S. T. Pantelides, "Theory of inelastic multiphonon scattering and carrier capture by defects in semiconductors: Application to capture cross sections", Phys Rev B **92**, 214111 (2015).
[70] G. Kresse, and D. Joubert, "From ultrasoft pseudopotentials to the projector augmented-wave method", Phys Rev B **59**, 1758 (1999).
[71] M. Shishkin, and G. Kresse, "Implementation and performance of the frequency-dependent GW method within the PAW framework", Phys Rev B **74**, 035101 (2006).
[72] S. Lany, "Band-structure calculations for the 3d transition metal oxides in GW", Phys Rev B **87**, 085112 (2013).
[73] S. Lany, "Semiconducting transition metal oxides", J Phys-Condens Mat **27**, 283203 (2015).
[74] P. Jackson, R. Wuerz, D. Hariskos, E. Lotter, W. Witte, and M. Powalla, "Effects of heavy alkali elements in Cu(In,Ga)Se2 solar cells with efficiencies up to 22.6%", physica status solidi (RRL) – Rapid Research Letters **10**, 583 (2016).
[75] W. Wang, M. T. Winkler, O. Gunawan, T. Gokmen, T. K. Todorov, Y. Zhu, and D. B. Mitzi, "Device Characteristics of CZTSSe Thin-Film Solar Cells with 12.6% Efficiency", Adv Energy Mater **4**, 1301465 (2014).
[76] F. W. de Souza Lucas, A. W. Welch, L. L. Baranowski, P. C. Dippo *et al.*, "Effects of Thermochemical Treatment on CuSbS2 Photovoltaic Absorber Quality and Solar Cell Reproducibility", The Journal of Physical Chemistry C **120**, 18377 (2016).
[77] A. W. Welch, L. L. Baranowski, P. Zawadzki, C. DeHart, S. Johnston, S. Lany, C. A. Wolden, and A. Zakutayev, "Accelerated development of CuSbS2 thin film photovoltaic device prototypes", Prog Photovoltaics **24**, 929 (2016).
[78] A. W. Welch, L. L. Baranowski, P. Zawadzki, S. Lany, C. A. Wolden, and A. Zakutayev, "CuSbSe2 photovoltaic devices with 3% efficiency", Appl Phys Express **8**, 082301 (2015).
[79] T. Kirchartz, J. Mattheis, and U. Rau, "Detailed balance theory of excitonic and bulk heterojunction solar cells", Phys Rev B **78** (2008).
[80] M. A. Green, "Radiative efficiency of state-of-the-art photovoltaic cells", Prog.Photovolt.: Res.Applic. **20**, 472 (2012).
[81] U. Rau, B. Blank, T. C. M. Muller, and T. Kirchartz, "Efficiency Potential of Photovoltaic Materials and Devices Unveiled by Detailed-Balance Analysis", Phys Rev Appl **7** (2017).
[82] R. E. Brandt, V. Stevanovic, D. S. Ginley, and T. Buonassisi, "Identifying defect-tolerant semiconductors with high minority-carrier lifetimes: beyond hybrid lead halide perovskites", Mrs Commun **5**, 265 (2015).
[83] W.-J. Yin, T. Shi, and Y. Yan, "Unusual defect physics in CH3NH3PbI3 perovskite solar cell absorber", Appl Phys Lett **104**, 063903 (2014).